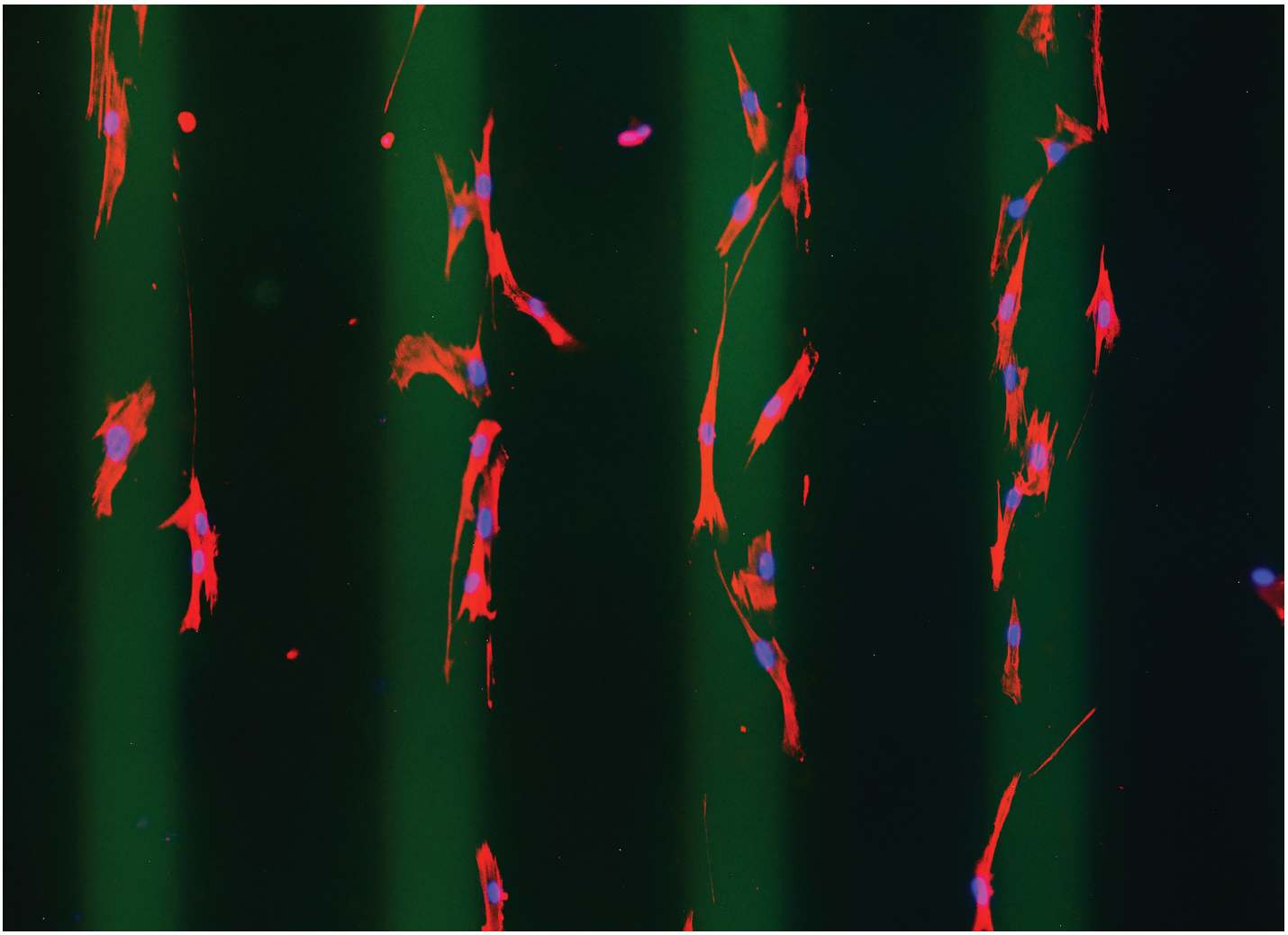

Highlighting a research work from the Disease Bioengineering Lab at the University of Utah, USA.

A soft-stiff patterned bioengineering model reveals kinase pathways driving directional cell migration in pulmonary arterial hypertension

This study introduces a patterned "zebra-crossing" hydrogel that mimics the mechanical landscape of pulmonary arterial hypertension (PAH). When exposed to alternating soft–stiff stripes, PAH smooth muscle cells migrate directionally—revealing a stiffness-guided behavior regulated by JAK/STAT signaling. These findings highlight druggable kinase pathways behind mechanosensitive migration and open new avenues for targeting stiffness-driven vascular disease.

Image reproduced by permission of Taslim A. Al-Hilal from *Biomater. Sci.*, 2025, **13**, 5671.

As featured in:

See Taslim A. Al-Hilal *et al.*, *Biomater. Sci.*, 2025, **13**, 5671.

ROYAL SOCIETY OF CHEMISTRY

rsc.li/biomaterials-science

Registered charity number: 207890

Biomaterials Science

ROYAL SOCIETY OF CHEMISTRY

PAPER

View Article Online
View Journal | View Issue

Cite this: *Biomater. Sci.*, 2025, **13**, 5671

A soft-stiff patterned bioengineering model reveals kinase pathways driving directional cell migration in pulmonary arterial hypertension

Tamanna Islam,[a] Jacob Hooper,[b] Xiaojun Zhang,[b] Clarissa Garcia,[b] Md Mahedi Hasan,[a] David H. Drewry,[c,d] Mohammad Anwar Hossain *[c] and Taslim A. Al-Hilal *[a,e]

Directional cell migration by pulmonary arterial cells (PACs) is one of the important features of diseases involving arterial remodeling, such as pulmonary arterial hypertension (PAH), a disease that is often characterized by reduced arterial compliance and increased extracellular matrix (ECM) stiffening. However, there are no therapeutics that can halt the directional cell migration of PACs in PAH. The inability to identify drug targets or drugs against the directional cell migration during PAH pathogenesis stems from an incomplete understanding of the process and a lack of effective translational models for screening of candidate small molecules. Here, for the first time, we introduce a bioengineered platform suitable for screening small molecule inhibitors targeting kinase pathways that are potentially linked to ECM-mediated directed cell migration in PAH. We used a photolithographic technique to develop mechanically patterned hydrogels with alternative stripes of soft and stiff bars representing the alternating stiffness regions of PAH ECM. Employing our bioengineered platform, we demonstrated the directional cell migration capacity of PACs and found that PAH-smooth muscle cells (SMCs) showed the highest ability to migrate from soft-stiff regions. Screening of different kinase inhibitors identified the role of JAK/STAT as a mechanosensor in the PAH-SMC-specific directional cell migration. Our study highlighted the use of a mechanically patterned bioengineering platform to identify new drug targets specific to the machinery involved in directional cell migration in PAH.

Received 13th February 2025,
Accepted 25th August 2025

DOI: 10.1039/d5bm00224a

rsc.li/biomaterials-science

1. Introduction

Pulmonary arterial hypertension (PAH) is a rare disease that affects people of all ages and genders. If left untreated, PAH patients die within ~12 months of diagnosis, with only a 45% survival rate after 3 years of diagnosis.[1,2] Pathological recruitment of arterial cells to sites of vascular remodeling and subsequent activation or dedifferentiation are critical steps in the progression of PAH.[2] During remodeling, excessive extracellular matrix (ECM) deposition causes fibrosis, while uncontrolled proliferation and migration of pulmonary cells result in higher pulmonary resistance and muscularization (presence of PAH-SMCs in the distal arterioles).[3,4] The excessive buildup of matrix components leads to spatiotemporal variations in ECM stiffness that can significantly influence regular cellular activity.[5] Cell phenotypes in PAH are substantially impacted by the changes in the stiffness and content of ECM, shifting from a contractile non-disease phenotype to a migratory synthetic disease phenotype.[6] Recent progress in developing bioengineered matrices with stiffness variations has facilitated the study of cell migratory phenotype *in vitro*,[7–11] demonstrating various forms of directional cell migration capacity of stem cells, tumor, stromal, vascular, epithelial, and immune cells. Despite the demonstration of the directional migration of various vascular cells, there are no tools to identify potential drug targets or screen compound sets against the directional cell migration of PAH.

The first pathological alteration that occurs at the beginning of PAH is early-stage small pulmonary arterial stiffening, which sets off mechanobiological remodeling at the distal arterioles.[12] The mechanical stiffness progressively increases from distal-to-proximal arteries, ranging from 1–10 kPa, and is

[a]*Department of Biomedical Engineering, University of Utah, Salt Lake City, Utah, USA. E-mail: taslim.al-hilal@pharm.utah.edu*
[b]*Department of Biological Sciences, College of Sciences, University of Texas El Paso, El Paso, Texas 79968, USA*
[c]*SGC-UNC, University of North Carolina at Chapel Hill, Chapel Hill 27599, USA. E-mail: anwar.hossain@unc.edu*
[d]*UNC Lineberger Comprehensive Cancer Center, School of Medicine, University of North Carolina at Chapel Hill, USA*
[e]*Department of Molecular Pharmaceutics, University of Utah, Salt Lake City, Utah, USA*

often elevated in severe PAH.[12] Cells respond to this mechanical perturbation due to the changing ECM stiffness and subsequently activate the signaling molecules involved in detecting stiffness-induced mechanotransduction, a process controlled by integrins and several kinases, *e.g.*, focal adhesion kinases, JAK/STAT kinases, and hippocampal signaling networks.[13–15] During PAH, endothelial cells (ECs), smooth muscle cells (SMCs), and pericytes migrate from their own layer to different layers and cause arterial remodeling.[16,17] Pulmonary arteriole sections are usually classified as proximal, middle, and distal segments and are defined based on the diameter of the arterial lumen. Their diameter varies from >75 to (75–25) to <25 μm, and both proximal and middle regions consist of layers of SMCs, whereas the distal section extending from the middle to capillaries only contains a single layer of ECs. SMCs are known to cross the border, muscularize distal arteries, and subsequently proliferate, which leads to vascular remodeling.[15,16,18–20] While several biochemical factors are known to regulate the movement of PAH cells,[20] our understanding of the involvement of mechanosensors in PAH arterial remodeling is still unclear. To better understand cellular mechanobiology, several attempts have been made over the last two decades to create cell culture substrates with mechanically defined matrix rigidity that mimics natural tissue stiffness throughout healthy and diseased situations. Nevertheless, we are still lacking tools that can be used to study the stiffness-induced directional migration of PAH cells and that allow us to screen for compounds that can halt the activation of mechanosensors and the movement of PAH cells before arterial remodeling.

Overall, we are still lacking tools that can be used to study the stiffness-induced directional migration of PAH cells and that allow us to screen for compounds that can halt the activation of mechanosensors and the movement of PAH cells before arterial remodeling. To this end, in this work, we have created a hydrogel-based bioengineered model with an alternating matrix stiffness lining to investigate the directional cell migration of pulmonary arterial cells taken from PAH patients, namely endothelial cell (PAH-EC), smooth muscle cell (PAH-SMC), and adventitial cell (PAH-ADC). The migration index of each PAH cell type was established. Based on the assessment of the cell migration in the soft-stiff patterned model, we screened a wide range of small-molecule kinase inhibitors (KIs) to identify the kinases (mechanosensors) involved in the directional cell migration of PAH cells.

2. Methods

2.1. Key cell line

The primary pulmonary arterial cell lines used were normal endothelial cells (N-ECs), N-SMCs, fatal donor adventitial cells (FD-ADCs), PAH-ECs, PAH-SMCs, and PAH adventitial fibroblast cells (PAH-ADCs). The N-ECs, N-SMCs, and PAH-ADC were obtained from both healthy male and female donors. The PAH-stemmed ECs, SMCs, and ADCs were obtained from both male and female patients who were diagnosed with idiopathic pulmonary arterial hypertension. All cells were acquired from the Pulmonary Hypertension Breakthrough Initiatives (PHBI) specimen bank (**https://www.ipahresearch.org**) and used as provided. All experiments were performed in accordance with the guidelines of the ethical standards of the University of Utah Institutional Review Board (IRB). As the cells were obtained from an external biorepository, the study was reviewed for compliance with University of Utah's policies on human tissue transfer and use of de-identified biospecimens. A Material Transfer Agreement (MTA) was executed through the University of Utah's PIVOT Center, ensuring that the use of these samples adhered to all applicable federal, state, and institutional regulations. No identifiable donor information was accessed or used in this study, and all data were handled in accordance with HIPAA and University of Utah IRB guidelines. The cells were stored in liquid nitrogen upon receiving. MV2 and Vasculife-SMC growth medium with 10% supplement and 1% antibiotic were used for cell culturing. For all experiments, passages 3–6 were used.

2.2. Step-by-step preparation of the micropatterned soft/stiff gel platform

2.2.1. Preparation of the quartz-based micropatterned array (master mold). The micropatterned array model (master mold) consisting of 200 μm stripes, each separated by a 100 μm distance, was designed using AutoCAD (Autodesk). The model was transferred to a chrome-covered quartz transparency mask using high-resolution printing (Advance Reproductions Corporation, MA) following photolithography techniques. This photolithographically patterned microarray structure was later used to create soft-to-stiff gel patterns on the 12 mm diameter glass coverslips.

2.2.2. Pretreatment of glass slide and coverslips. Prior to the preparation of the alternating gel pattern, the glass slides that were used to attach coverslips for soft gel coating underwent rigorous pretreatment processes. The glass slides were initially soaked in 5% Dimethyldichlorosilane (DMC) solution for 15 minutes, followed by drying at RT for 20 minutes and removing excess DMC through washing with methanol. This pretreatment produced an oily coating on the glass surface necessary for easily detaining the coverslips. This pretreated glass slide can also be reused as many as ten times for coverslip attachment before it loses the DMC coating.

Glass coverslips were initially UV-treated for 5 minutes on each side using a UVP Transilluminator (Bio-Rad, CA). A solution of 1% methacrylate was prepared by mixing 200 μL methacrylate, 600 μL of acetic acid (initially diluted in deionized water at a ratio of 10 : 1), and 20 mL of 100% ethanol. After UV curing, the coverslips were soaked in the methacrylate solution for 5 minutes, then washed with absolute ethanol twice and dried using high-purity nitrogen. Once the coverslips were dried, these were used for soft gel coating.

2.2.3. Preparation of soft gel layer. A solution of polyacrylamide gel with an expected stiffness of 1 kPa was prepared following a previously prepared protocol.[21] Briefly, a mixture of

200 μL 2% bis-acrylamide (0.4%) (Thermo Fisher Scientific, Inc., USA), 100 μL of 40% acrylamide solution (4%) (Thermo Fisher Scientific, Inc. USA), and 700 μL PBS was prepared. Then 5% of UV active IrgaCure® (Sigma-Aldrich, Inc., MO) (w/v – 0.05 mg mL^{-1} in ethanol) was added to the solution. Once the solution was ready, a 9 μL of the solution was drop-casted on the pretreated glass slide. The pretreated coverslips were then carefully placed on the glass slide containing the gel drop. The solution was spread evenly throughout the entire coverslip placed on the glass slide due to fluid tension between the glass slide and the cover slip. Once the coverslips were placed, they were exposed to UV light for 7–10 minutes for gel polymerization. After UV exposure, a razor blade was used to detach the coverslips from the glass slide carefully. The coverslips were then placed in a heater with the gel side facing upward and heated at 30 °C for 30 minutes.

2.2.4. Preparation of stiff gel pattern. A solution of polyacrylamide gel of stiffness 10 kPa was prepared following the same protocol.[21] Briefly, a solution of 200 μL 2% bis-acrylamide (0.4%), 120 μL of 40% acrylamide solution, and 680 μL PBS were prepared in which 1% of IrgaCure® (w/v – 0.05 mg mL^{-1} in ethanol) was added. A 9 μL gel solution was added to the micropatterned array (master mold). The soft gel-coated coverslips were then carefully placed onto the drop with the gel side facing down so no bubbles were created between the glass side and the coverslips. The gel was then UV-cured for 7–10 minutes. After UV curing, 1 mL of PBS was added on top of the coverslips; then, using the razor blade, the coverslips were gently detached and peeled off from the master mold. The pre-made soft/stiff gel-coated coverslips were washed twice with sterile PBS to remove the excess uncured gel. The final soft/stiff gel-coated coverslips were stored in 24 wells at 4 °C containing PBS until further use.

2.2.5. Preparation of collagen I embedded soft and stiff gel. A 100 μg mL^{-1} of collagen I was added in the soft and stiff gel solutions to prepare the collagen embedded gels. To get this concentration 29 μL of collagen I was added in both soft and stiff gels from a 3.47 mg mL^{-1} collagen I (Corning®, USA) solution. For the soft gel briefly, a mixture of 200 μL 2% bis-acrylamide (0.4%) (Thermo Fisher Scientific, Inc., USA), 100 μL of 40% acrylamide solution (4%) (Thermo Fisher Scientific, Inc. USA), 29 μL collagen I (Corning®, USA), and 671 μL PBS was prepared. Then 5% of UV active IrgaCure® (Sigma-Aldrich, Inc., MO) (w/v – 0.05 mg mL^{-1} in ethanol) was added to the solution. For the stiff gel briefly, a solution of 200 μL 2% bis-acrylamide (0.4%), 120 μL of 40% acrylamide solution, 29 μL collagen I (Corning®, USA), and 651 μL PBS were prepared in which 1% of IrgaCure® (w/v – 0.05 mg mL^{-1} in ethanol) was added. The gels were prepared on cover slides following the protocol described in previous sections (sections 2.2.3 and 2.2.4).

2.6. Directed cell migration assay

A 10 mM solution of sulfo-SANPAH (Thermo Fisher Scientific, Inc., USA) was prepared and added to the wells to activate the gel surface for cell seeding. Then, the coverslips were exposed to UV light for 15 minutes. After UV exposure, the sulfo-SANPAH solution showed a visible color change from purple to red, indicating complete UV curing. After the sulfo-SANPAH treatment, the solution was aspirated, and the wells were washed with sterile PBS until all residue color disappeared. A 10 μg mL^{-1} collagen type I solution was prepared in sterile PBS and added to a new 24 wells, 500 μL each. After washing, the coverslips were carefully transferred to the new 24 wells containing collagen solution using a tweezer with the gel side facing upward. Afterward, the coverslips were incubated overnight in collagen solution before cell seeding. Before cell seeding in the soft/stiff gel platform, cells were cultured in their respective media in polystyrene flasks. When the cell confluency reached 70–80%, they were trypsinized and counted. Approximately 1500–5000 cells were seeded per well containing the micropatterned soft/stiff gel-coated coverslips. After 24 hours of cell seeding, growth media was carefully aspirated without touching the gel, and 4% paraformaldehyde (PFA) was added to the wells. After 20 minutes of cell fixation with PFA, the solution was removed and washed with PBS twice. Next, the coverslips were incubated with cell permeabilization buffer (0.5% TritonX in PBS) for 15 minutes at 4 °C and washed once. The coverslips were then incubated with a blocking buffer (53% bovine serum albumin BSA in PBS) for 45 minutes at 4 °C. After blocking, the coverslips were washed once with PBS. A diluted solution of phalloidin (5 μL in 500 μL of PBS with 1% PBS) was added to the well and incubated for 30 minutes in a covered container at RT. After staining, the solution was carefully aspirated and washed twice with PBS. Finally, the coverslips were mounted on the glass slides using DAPI mounting media with the gel side facing down and imaged.

2.7. Directed cell migration assay for whole coverslip

After 22 hours of cell seeding to the 24 wells containing the gel-coated coverslips, the PAH-SMCs were incubated with CellTracker™ green CMFDA dye (Invitrogen™, USA) (with growth media) for 2 hours. Afterward, the cells were washed with PBS twice to remove excess dye and fixed with 4% PFA for 20 minutes at 4 °C. After fixation, the coverslips were washed once with PBS and mounted on the glass side for imaging.

2.8. Radial plot

Percentage of cells *vs.* angle (radial plot) was plotted to determine the angular distribution of cells with respect to the stiff bars. The angle of each cell was measured against the stiff bar representing vertical 90 degree. The closer the angle value to 90 degrees, the better the directionality toward stiff gel.

2.9. JAK3 siRNA transfection

JAK3 siRNA (JAK3 Human siRNA Oligo Duplex, Locus ID 3718, OriGene Inc. USA) transfection in PAH-SMCs was obtained by following the manufacturer protocol. Briefly, the lypholized siRNA was reconstituted in sterilized duplex buffer supplied by the manufacturer. Approximately 50 nM siRNA was prepared by diluting the stock siRNA in 1× transfection buffer (cat# TT320001)

supplied by the manufacturer. Before adding to the cell, cells were freshly seeded in a 6 well plate (100 000 cells per well). After 24 hours of cell seeding, the diluted siRNA solution with optimum amount of transfection agent (Trans 2.0, cat#TT320001, OriGene Inc.) was added. After 24 hours of post transfection, the cells were collected and seeded on the micropatterned platform for studying directional cell migration. For control, cells were given scrambled siRNA, diluted in transfection buffer following the same method mentioned above.

2.10. qRT-PCR

RNA extraction was conducted using the TRIzol reagent (Thermofisher, Cat# 15596026), yielding samples with A_{260}/A_{280} ratios between 2.0 and 2.10. The extracted RNA was then reverse transcribed into cDNA utilizing the AccuPower® RocketScript™ Cycle RT PreMix (Bioneer, Cat# K-2201), following the manufacturer's protocol for the BIO-RAD CFX96 C1000 system. To evaluate relative mRNA expression levels, RT-PCR was performed using the Applied Biosystems™ PowerUp™ SYBR™ Green Master Mix (Applied Biosystems™, Cat# A25742) on the BIO-RAD CFX96 C1000 q-PCR system. The primer sequences utilized are human JAK3 gene (F = CCA GAT GGA AAC TGT TCG CTC AG and R = GAG GTT GGT ACA TCA GAA ACA CC) and housekeeping gene GAPDH (F = GTC TCC TCT GAC TTC AAC AGC G, and R = ACC ACC CTG TTG CTG TAG CCA A). Data analysis was performed using Prism – GraphPad version 9.5.0, utilizing Welch's test for comprehensive statistical evaluation.

2.11. Cytotoxicity study

We employed live and dead cell imaging kits (Thermo Fisher Scientific) to determine the number of live and dead cells after KI treatment. The assay was performed following the company's instructions. Briefly, both green (A) and red vials (B) were thawed and mixed. After the KI treatment with various concentrations, the mixture of A and B was added to the cell and incubated for 15–20 minutes. After incubation, cells were imaged under the microscope.

2.12. Anti-migration assay for drug screening

Initially, a 10 mM concentration of KIs was prepared in DMSO and stored at 20 °C before use. The working KIs were diluted from the stock concentration in the growth media. The dilutions were carefully made so the volume of DMSO was as minimal as possible in the wells. After seeding cells in the wells, the growth media containing the KI was added to the wells and incubated for 24 hours. Afterward, the cells were washed once with PBS to remove the KIs, fixed, permeabilized, blocked, and stained with phalloidin using the same instructions discussed in the directed cell migration assay section. Then, the coverslips were mounted on glass slides for imaging.

2.13. Single gel preparation

Single soft/stiff gel-coated coverslips (25 mm diameter) with expected Young's modules of 1 and 40 kPa were prepared following the previously published protocol.[22] Briefly, a solution of 1 kPa stiffness was prepared by mixing 750 μL of 40% acrylamide, 500 μL of 2% bis-acrylamide, 100 μL of 10% APS, and 10 μL of TEMED in DI to make a 10 mL solution. For the solution of stiffness 40 kPa, a mixture of 2 mL of 40% acrylamide, 2.4 mL of 2% bis-acrylamide, 100 μL of 10% APS, and 10 μL of TEMED was prepared in DI to make a 10 mL solution. Then 13 μL of the respective solution was drop-casted on the pretreated glass slide upon which coverslips (after treating with methacrylate solution) were placed. Then the solution was allowed to spread through the entire coverslip. Then the gel was allowed to polymerize at RT. Once the gel was formed, the coverslips were carefully detached from the glass slide using a tweezer and stored in a 6-well plate containing sterile PBS at 4 °C before further use. Before cell seeding, the coverslips were sterilized under UV for 5 minutes and then incubated with collagen (10 μg mL^{-1}) solution overnight. After incubation, the collagen solution was carefully aspirated, and cell suspension was added for culturing.

2.14. Western blot analysis

The cell lysate from single gel-cultured PAH-SMCs was prepared using the lysis buffer and protease inhibitor. Depending on the molecular weight of the protein, a 7.5% concentrated polyacrylamide gel was used for protein separation from the cell lysates. Approximately 20–70 μg protein (20 μg for GAPDH, 30–50 μg for STAT3, and 70–80 μg for JAK3) was loaded onto the gel. The protein concentration in the cell lysate was calculated using a BCA protein quantification assay (Pierce, ThermoFisher, CA). The absorbance was recorded at 594 nm using a synergy MX2 plate reader (Bio-Tek, Burlington, VT). After separating the protein loaded on the gel *via* electrophoresis, the samples were transferred to 0.45 μm polyvinylidene difluoride (PVDF) membranes (IPVH00010, Millipore). Afterward, the membranes were blocked in 5% BSA (in TBST buffer) for one hour. Then, the membrane was incubated in their respective primary antibody solution with a dilution of 1 : 1500, which was prepared in a 5% BSA solution. The antibodies used are anti-JAK3 (#8827s, Cell Signaling Technology Inc.), anti-phospho JAK3 (#5031, Cell Signaling Technology Inc.), anti-STAT3 (#12640, Cell Signaling Technology Inc.), anti-phospho STAT3 (#9145, Cell Signaling Technology Inc.), and anti-GAPDH (#MAB5718SP, R&D Systems, Inc.). Afterward, the membrane was washed with TBST buffer three times and incubated with the respective HRP conjugated secondary antibody (mouse IgG HRP, #HAF018, and rabbit IgG HRP, #HAF008, R&D Systems, Inc.) with dilution 1 : 2000 in 5% BSA blocking buffer. The membranes were then incubated with WesternSure® Enhanced Chemiluminescent substrate (LI-COR Biosciences, Lincoln, NE) for 1 minute and visualized using a ChemDoc XRS System (Bio-Rad Laboratories, Hercules, CA).

2.15. Statistical analysis

We performed the statistical analysis at $\alpha = 0.05$ (95% confidence interval) with GraphPad Prism (version 10.02, GraphPad Software, San Diego, CA) using *t*-test as applicable.

3. Results

3.1. Development of micropatterned soft/stiff bioengineering model

To investigate the process of stiffness-directed cell migration influenced by the altering ECM, we designed a photolithographically lined polyacrylamide-based hydrogel system as a model ECM, consisting of 100 μm width stripes, each stamped 200 μm apart (Fig. 1). Initially, we designed a base micropatterned array using photolithography technique (Fig. 1A). Later, we UV-polymerized a polyacrylamide solution (PA1, 1 μg mL^{-1}, 1 kPa) on a 12 mm pre-treated coverslip, followed by incubation at 30–35 degrees for 30 minutes. Then, using the predesigned micropatterned array, a second polyacrylamide solution (PA2, 10 μg mL^{-1}, 10 kPa) was UV-crosslinked on the soft gel layer and, thus, created alternating stripes of soft-stiff gels over an approximate distance of 200 μm (Fig. 1B). The final model consisted of mechanically patterned "step" gels consisting of soft and stiff stripes with widths of 200 μm and 100 μm, respectively. Once the soft/stiff stripes were lined and crosslinked, we carefully removed the coverslips from the photomask and stored them in 24 wells for the directional cell migration assay. Our platform allows the analysis of 24 samples simultaneously, making it highly efficient and suitable for low throughput screening of inhibitors that can affect directed cell migration.

3.2. Stiffness promotes directional PAH cell migration in soft/stiff patterned gel

In PAH, arterial remodeling is characterized by the migration of ECs, SMCs, and ADCs. To understand if the changes in ECM rigidity cause directional cell movement of PAH cells, we used our soft/stiff patterned model. We studied the directional cell migration of four distinct arterial cells: normal and PAH endothelial cells: N-ECs, PAH-ECs; smooth muscle cells: N-SMCs, PAH-SMCs; and adventitial cells: N-ADCs, PAH-ADCs collected from different patients (Table S1). The capability of cells to migrate from soft-to-stiff stripes was assessed after 24 hours of cell seeding, and the directional migration index (DMiX) was determined by quantifying the number of cells accumulated on the stiff *versus* soft stripes based on the color profile of the pre-labeled cells (Fig. 2A). The higher the DMiX value, the stronger the cell migration from soft-to-stiff hydrogels. While we observed some patient-to-patient variability among the PAH cell types, PAH-ECs seemed to have the lowest and comparable DMiX than their healthy counterparts (Fig. 2B and C). On the other hand, PAH-SMCs and PAH-ADCs showed higher DMiX than their controls despite having some patient variability (Fig. 2D and E). Among different PAH cell types, we found that PAH-SMCs showed the highest DMiX (Fig. 2F). To further confirm, we have also analyzed the radial plot of angular distribution for each cell variable (Fig. 2G). The center of each stiff bar was chosen for determining the angular position of the cells, with the stiff bar as the vertical 90-degree orientation (along the *Y* axis). Approximately 20 positions, 5 positions for each stiff bar, were selected for cellular angle determination. We observed that the PAH-SMCs mostly aligned at 90° while N-ECs and PAH-ECs exhibited randomized angular distribution. PAH-ADCs also demonstrated profound alignment remaining at 90°. These results demonstrate the directional migration of PAH-cells, where PAH-SMCs show the highest migration along with stiffness.

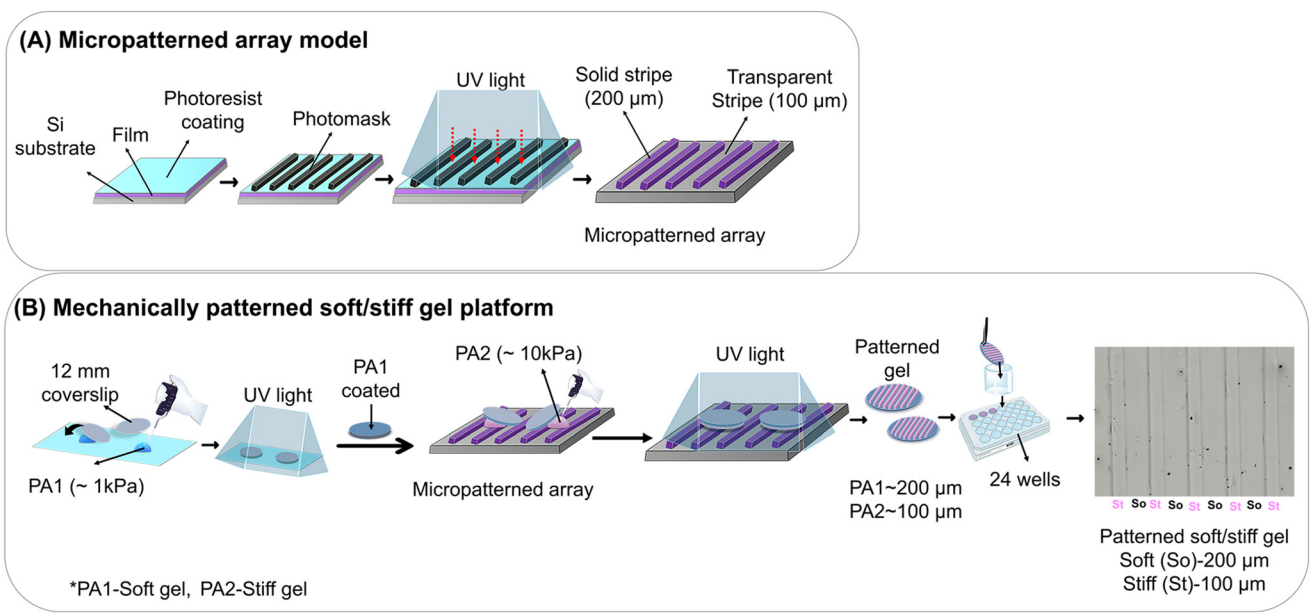

Fig. 1 Development of micropatterned soft/stiff gel platform. (A) Schematics showing how the micropatterned arrays were designed. (B) Stepwise design of hydrogel-based soft/stiff gel lining using the micropatterned array model.

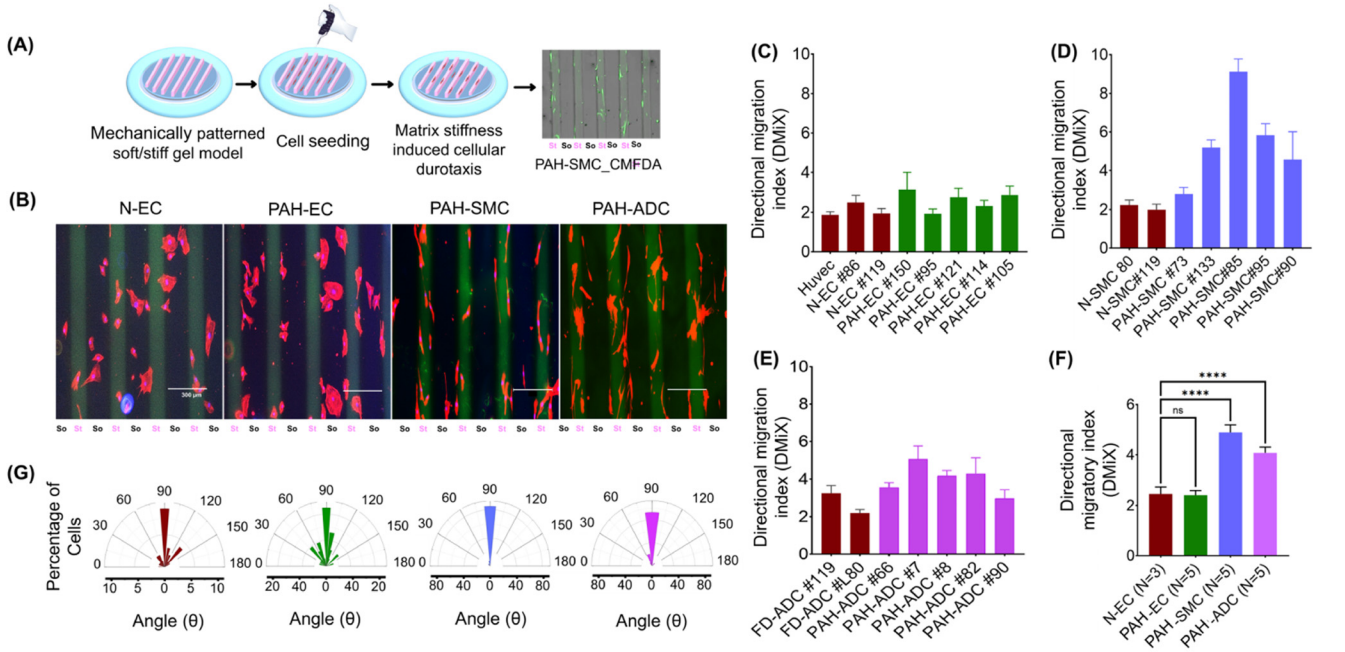

Fig. 2 Investigation of the DCM of pulmonary arterial cells using the soft/stiff gel platform. (A) Schematics showing the steps followed while performing DCM. (B) Microscopic images recorded after 24 hours of cell incubation for four different cells (red-phalloidin, blue-DAPI, green-background). (C, D, and E) The plot of DMiX *vs.* the type of cells: HUVEC, healthy donor-derived ECs, SMCs, ADC, and PAH patient-derived ECs, SMCs, and ADCs. (F) Bar plot showing the DMiX of the cells (N-EC, PAH-EC, PAH-SMC, and PAH-ADC) obtained after DCM. (G) Radial plot showing the angular distribution of cells (shown in B) from the stiff bar (n = 20) (p-values calculated using Kruskal–Wallis test; *p < 0.05, **p < 0.01, ***p < 0.001, and ****p < 0.0001).

With a goal in mind to screen compounds, we set up a robust semi-automated method to facilitate the calculation of the DMiX using a simplified process. Pre-labeled cells can be imaged right after the time point (24 hours of incubation) without performing the cell staining process. Initially, we confirmed the migration efficiency of PAH-SMCs for different cell densities ranging from 1500 to 5000 cells per well. We observed no differences in the DMiX values across all cells counts and staining methods (Fig. S1). Next, we analyzed the entire patterned gel by taking images of seven different regions at a lower magnification. We received similar results demonstrating that PAH-SMCs exhibited stiff ECM-directed migration throughout the entire patterned structure (Fig. S2), resulting in almost unidirectional movement from soft-to-stiff stripes. This also substantiates our bioengineered model's validity for studying cell-specific ECM stiffness-directed migration. We utilized collagen type I containing acrylamide gel with two different stiffness mimicking real ECM composition to study cellular migration. Our observations showed no difference in the directional migration of PAH-SMCs, regardless of the presence or absence of collagen (Fig. S3). Our results indicate that ECM stiffness alone is a key factor in adhesion formation, as cells tend to form larger adhesions on stiffer surfaces. This variation in adhesion strength, driven by increased actomyosin contractility, may promote migration from softer to stiffer substrates, thereby influencing directional cell movement.[23–25]

3.3. Screening of kinase inhibitors using the soft/stiff patterned gel

Cell migration is known to be modulated by many kinases that are activated at the focal adhesion sites, assisting the movement of cells from one location to another. To investigate the effects of different kinase pathways in ECM stiffness-directed cell migration, we screened a wide range of KIs targeting JAK/STAT, STK3/MST2, Rho kinase, and TBK1 based on their known role in PAH pathology and cellular migration.[26–28] Utilizing our assay method that employs our soft/stiff patterned model, we screened 21 compounds to study their inhibitory effects on the DMiX of PAH-SMCs (Fig. 3A and Table S2). All the compounds were screened at 1 μM concentration. After 24 hours of plating with KIs, PAH-SMCs were immediately imaged, and DMiX was calculated. If the median DMiX value of any KI had a similar value to that of the N-SMCs, which is less than 2 (cutoff), we considered that as a hit compound. Several KIs targeting the JAK/STAT pathway (JAK3-in-6 and PF06700841 inhibitors) and the STK/MST pathway (UNC-BE4-017, UNC-BE4-018, UNC-BE4-040, and XMU-MP-1) showed DMiX lower than the cutoff (Fig. 3B, Fig. S4 and Table 1). Our results identify JAK/STAT and MST2 kinases as mechanosensors that may be involved in the ECM-stiffness-directed migration of PAH-SMCs.

We focused on the JAK/STAT pathway targeting JAK-in-6 and PF06700841 inhibitors for downstream anti-migration analysis of PAH-SMCs (Fig. 3C). Fig. 3D demonstrates the representative

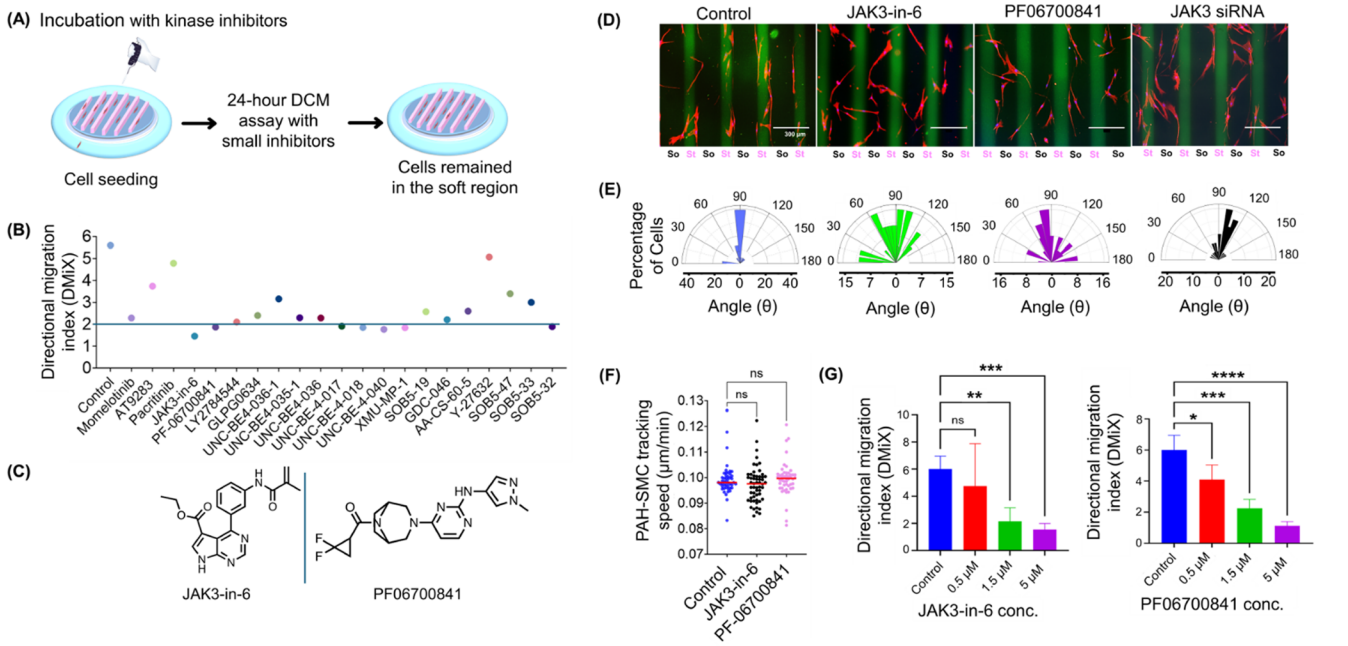

Fig. 3 Study of the molecular kinase pathways associated with the DCM of PAH-SMCs using kinase targeting small molecules. (A) Schematics representing the steps involved in the treatment process with kinase targeting small molecules in the DCM of PAH-SMCs. (B) Dot plot showing the DMiX obtained after treating PAH-SMCs with 21 different small molecules targeting JAK3/STAT3, Hippo, and Rock kinase pathway. (C) The chemical structures of JAK3-in-6 and PF06700841 inhibitors. (D) Representative microscopic images showing the DCM of PAH-SMCs for control, JAK3-in-6, PF06700841 compounds, and JAK3 siRNA treated PAH-SMCs (red-phalloidin, blue-DAPI, green-background). (E) Representative radial plots showing the angular distribution of PAH-SMCs (shown in D) before, after treatment with KIs, and siRNA treated PAH-SMCs (n = 20). (F) The cell trajectory plot obtained from live cell imaging for both treated (JAK3-in-6 and PF06700841) and untreated PAH-SMCs (G) DMiX values were obtained for treating PAH-SMCs with different concentrations of JAK3-in-6 and PF06700841 inhibitors (concentrations used: 0.5, 1.5, and 5 μM) (p-values calculated using Kruskal–Wallis test; *p < 0.05, **p < 0.01, ***p < 0.001, and ****p < 0.0001).

Table 1 List of inhibitors targeting JAK/STAT, STK/MST and STK3/MST pathways, the average DMiX, and IC_{50} values

Targeting pathway	Compounds	DMiX[a]	JAK1 (IC_{50})	JAK2 (IC_{50})	JAK3 (IC_{50})	Ref.
	Control	5.6 ± 1.8				
JAK/STAT kinase inhibitors	Momelotinib	2.29 ± 1.04	11 nM	18 nM	155 nM	56
	AT9283	3.74 ± 2.85	—	1.2 nM	1.1 nM	57
	Pacritinib	4.79 ± 1.72	1280 nM	23 nM	520 nM	58
	JAK3-in-6	1.46 ± 0.71	640 nM	1500 nM	0.15 nM	59
	PF06700841 (Brepocitinib)	1.87 ± 0.58	17 nM	77 nM	6.5 nM	60
	LY2784544 (Gandotinib)	2.1 ± 0.46	—	3 nM	48 nM	61
	GLPG0634 (Filgotinib)	2.4 ± 0.95	10 nM	28 nM	810 nM	62
	GDC-046	2.21 ± 0.84	0.7 nM	0.7 nM	0.4 nM	63
MST1/STK4 MST2/STK3 STK3/MST2 kinase inhibitor	UNC-BE4-036-1	3.16 ± 0.99	NT	124 nM		64
	UNC-BE4-035-1	2.3 ± 0.96	NT	7 nM		64
	UNC-BE4-036	2.29 ± 0.64	NT	NT		64
	UNC-BE4-017	1.91 ± 1.07	NT	41 nM		64
	UNC-BE4-018	1.85 ± 0.65	NT	195 nM		64
	UNC-BE-4-040	1.77 ± 0.54	NT	391 nM		64
	XMU-MP-1	1.84 ± 0.43	71.1 nM	38.1 nM		65
	UNC-SOB5-19	2.57 ± 0.72	NT	33 nM		64
	UNC-SOB5-47	5.07 ± 7.5	NT	28 nM		64
	UNC-SOB5-33	3.4 ± 1.9	NT	57 nM		64
	UNC-SOB5-32	1.89 ± 1.9	NT	142 nM		64
TBK1	AA-CS-6-005	2.24 ± 0.75	TBK1: IC_{50} = 100 nM			
Rho kinase inhibitor	Y-27632	2.6 ± 1.09	ROCK1: Ki = 200 nM			66

[a] DMiX = ratio of cells in the stiff to soft gel; IC_{50} = half-maximal inhibitory concentration; JAK1 = Janus kinase 1; JAK2 = Janus kinase 2; JAK3 = Janus kinase 3; STK = serine/threonine-protein kinase; MST = Mammalian STE20-like protein; NT = not tested.

images for directed migration of PAH-SMCs before and after compound treatment, indicating the inhibition of cell migration. Since JAK3-in-6 or PF06700841 may block kinases beyond JAK/STAT pathway, we tested the ability of directed migration in JAK3 knockdown PAH-SMCs. The siRNA-transfected PAH-SMCs exhibited a similar reduction in directional migration as observed with the kinase inhibitors (Fig. 3D and Fig. S5). Further analysis of cell alignment patterns confirmed the effective suppression of directional migration in both JAK3 knockdown cells and PAH-SMCs treated with these compounds (Fig. 3E). We next investigated the effect of kinase inhibitors on PAH-SMC's random motility through real time imaging for up to 24 hours. Neither JAK3-in-6 nor PF06700841 affected random motility of PAH-SMCs, as indicated by similar mean track speed and track length compared to the vehicle control (Fig. 3F, Fig. S6 and Videos S1–S3). The observed tracking speed of PAH-SMCs was consistent with previously reported findings.[16] Overall, our findings suggest that the JAK/STAT pathway primarily influences directed cell migration rather than the random motility of PAH-SMCs. Next, we investigated the dose dependent lowering of DMiX of two JAK/STAT KIs: JAK3-in-6 and PF06700841. To determine the dose dependency, we tested the DMiX of JAK3-in-6 and PF06700841 using three different concentrations at 0.5, 1.5, and 5 μM. The DMiX of each tested KI decreased with increasing concentrations (Fig. 3F and Fig. S7). These observations imply that the KIs are capable of exhibiting dose-dependent inhibition of the JAK/STAT pathway.

3.4. JAK3-in-6 and PF06700841 show drug-like properties with low cytotoxicity

JAK3-in-6 and PF06700841 have drug-like properties with appropriate lipophilicity (clog P), topological polar surface area (tPSA), and intrinsic solubility (log S) as well as potent inhibition (IC_{50}) for several Janus kinases. Both KIs have drug-like properties in generally accepted appropriate ranges, with MW < 400, clog P < 3.5, tPSA < 120, and log S > −3.25.[29,30] Both are potent JAK3 inhibitors, although JAK3-in-6 is more potent (IC_{50} = 0.15 nM) than PF06700841 (IC_{50} = 6.5 nM) for JAK3 (Table 1). The formation of stable microtubules is an important step for creating a strong focal adhesion, even for mitotic cell division, and KIs can exert their effect through the destabilization of microtubules, and this may be toxic to the cells at certain concentrations.[31] To determine the cytotoxicity of JAK3-in-6 and PF06700841, we treated the PAH-SMCs at four different concentrations (0.5, 5, 10, and 100 μM) at two time points (2 and 48 hours). DMSO (0.01%) was used as a vehicle control. We observed no cytotoxicity of JAK3-in-6 and PF06700841 at 2 hours: cell viability was above 90% at 100 μM (Fig. 4A and B). At 48 hours, both JAK3-in-6 and PF06700841 showed up to 75% of cell viability with the highest concentration. Importantly, up to 10 μM, none of the KIs showed any comparable toxicity at 2 and 48 hours (Fig. 4A and B). This result indicates that JAK3-in-6 and PF06700841 have drug-like properties and potent kinase inhibitory activity while exhibiting low toxicity for PAH-SMCs.

3.5. JAK3-in-6 and PF06700841 inhibitors suppress the stiffness-induced phosphorylation of JAK3 and STAT3

Different JAK/STAT isoforms are overactivated in pulmonary arterial cells of PAH arteries. Among Janus and other kinases, JAK3 had the highest phosphorylation pattern in human PAH-SMCs compared to N-SMCs.[26] While the role of the JAK2/STAT3 pathway in PAH has been studied, the activation of the JAK3/STAT3 pathway or other JAK isoforms is highly unknown

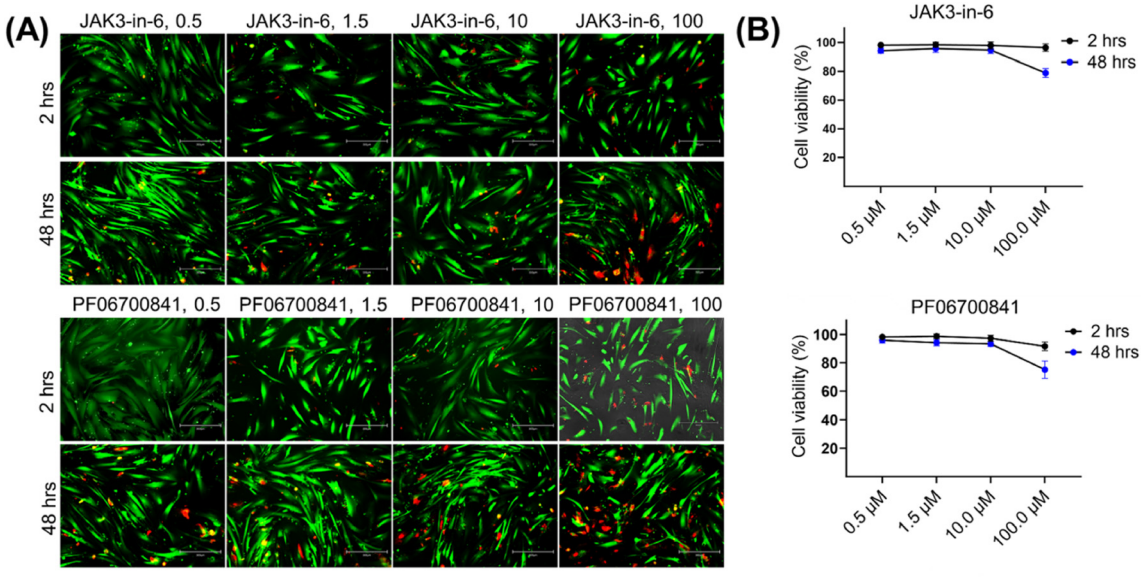

Fig. 4 Cytotoxicity study of JAK3-in-6 and PF06700841 inhibitors using different concentrations and times for incubation. (A) Microscopic images showing the number of live/dead cells obtained after treating cells with the respective inhibitors. Green-live and red-dead cells. (B) Cell viability percentage was obtained for different concentrations and incubation times.

in the context of stiffness-induced changes in PAH cells. Thus, we explored how the dynamics of JAK3/STAT3 activation changes due to stiffness and whether JAK3-in-6 and PF06700841 would effectively block the stiffness-induced JAK3/STAT3 activation. We first determined the phosphorylation patterns of JAK3 and STAT3 in PAH-SMCs after culturing them in Petri dishes, which are known to be very stiff, and treating the cells with JAK3-in-6 and PF06700841 at different concentrations and time points. The main objective of this experimental design was to optimize the time point and dose. Both JAK3-in-6 and PF06700841 effectively inhibited the phosphorylation of JAK3 and STAT3 only after 30 minutes of treatment (Fig. S8A and C). Although we observed some variations, the inhibition of JAK3 and STAT3 phosphorylation by JAK3-in-6 and PF06700841 was dose-dependent (Fig. S8B and D). We next aimed to understand how changing ECM stiffness influences the activation patterns of JAK3/STAT3 kinase that can be correlated with the directional migration of PAH-SMCs.

We cultured the PAH-SMCs in two different hydrogels with stiffness of 1 kPa (soft) and 10 kPa (stiff). Achieving 90% confluency, we treated the cells with JAK3-in-6 and PF06700841 and checked the phosphorylation of JAK3 and STAT3. Stiff gel induced higher phosphorylation of JAK3 and STAT3 than the soft gel (Fig. 5A and Fig. S9), indicating that increasing ECM rigidity can induce the activation of JAK3/STAT3 kinase. Moreover, JAK3-in-6 and PF06700841 reversed the phosphorylation of JAK3 and STAT3 in PAH-SMCs at a stiff gel that showed similar patterns with their basal level at soft gels (Fig. 5A and B). Our results suggest that JAK3-in-6 and PF06700841 have the potential to modulate the stiffness-induced changes of PAH-SMCs, and thus, they can be used to target the directional PAH-SMCs migration.

4. Discussion

Arterial remodeling is one of the main features of PAH where directional cell migration plays an important role. Pulmonary arterial muscularization is linked with SMC or pericyte migration from existing arteries. PAH-SMCs are also known to proliferate and migrate within their own medial layer and cause medial thickening. Our findings also confirm the ability of the vascular PAH vascular cells to be more responsive to directed cell migration driven by the ECM stiffness gradient. This behavior is largely driven by their elevated contractility and mechanosensitivity. Through actomyosin interactions, SMCs generate substantial traction forces, enabling them to detect and respond effectively to substrate stiffness.[32] Additionally, SMCs form stable focal adhesions, which support directional migration on stiffer matrices.[32] In contrast, ECs are more attuned to shear stress, adapting to hemodynamic forces within blood vessels.[33] ADCs reside in the outermost layer of blood vessels, known as the adventitia, where they contribute to vascular integrity by synthesizing collagen and other extracellular matrix components. In response to inflammatory stimuli or vascular injury, ADCs can undergo phenotypic transformation into myofibroblasts, a process marked by the expression of alpha-smooth muscle actin. This shift not only imparts contractile capabilities akin to SMCs but also enhances their migratory potential, enabling them to participate actively in vascular remodeling and repair.[34,35]

Another mechanical feature of PAH is the increased stiffening of arteries due to the deposition of excessive ECM. In PAH, ECM stiffening sustains cellular growth and induces migration by linking mechanical stimuli to the cell migratory machinery.[5,36] However, there are no targeted drugs that can

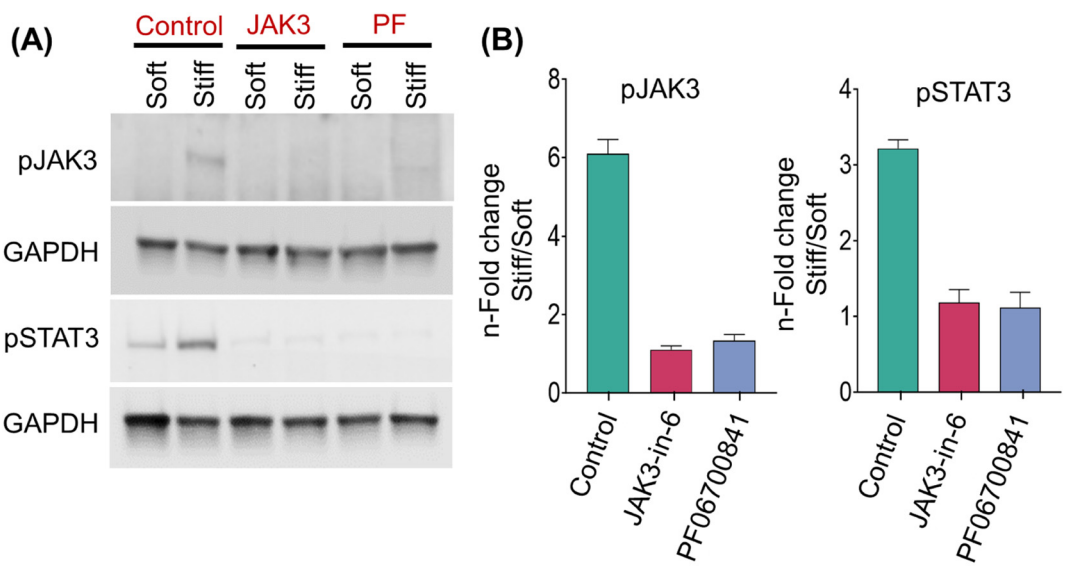

Fig. 5 (A) Western blot and (B) quantitative analysis of pJAK3 and pSTAT3 expressions obtained from PAH-SMCs cultured in soft *versus* stiff gels and treated with JAK3-in-6 (JAK3) and PF06700841 (PF) (5 μM, n = 3).

block the directional migration of PAH cells under different external stimuli, such as stiffness or hypoxia. Although the PAH animal models with genetic tools[37] and recently coined PAH-on-chip models[38,39] have greatly enhanced our understanding on the knowledge of specific facets of PAH-biology, there is no tool that allows for the study of the activation of different mechanosensors during directional migration of PAH cells or allows for compound screening against this phenotype. Our research adds to the growing body of literature on mechanically defined matrix rigidity-driven cellular mechanotransduction, which replicates the stiffness of natural tissues.[40] Various polymer materials, such as poly(ethylene glycol)-based artificial extracellular matrices and polydimethylsiloxane (PDMS) micropost arrays, have been developed to examine how matrix stiffness influences 3D cell migration, as well as migration under different confinement and surface coating conditions.[41,42] Hydrogel stiffness can be modulated by altering the precursor polymer concentration, allowing the creation of matrices with a range of mechanical properties. A collagen-based gel system has been used to study the effect of externally induced force gradients on angiogenic sprouting of human microvascular endothelial cells. Additionally, magnetic beads bioconjugated with collagen type I have been incorporated into the ECM to investigate mechanical signaling.[43] Among various gel systems, PA gels offer significant advances due to their chemical inertness and easily adjustable mechanical properties. By controlling acrylamide concentration, PAA gels can mimic the stiffness of natural tissues while maintaining biochemical consistency, as stiffness changes only affect gel crosslinking. Furthermore, PAA gels can be modified with natural ECM components such as collagen, laminin, fibronectin, and vitronectin to study integrin-dependent cell adhesion to the ECM. To this end, we created a micropatterned bioengineering model that consists of stripes with varying stiffness, which closely imitate the natural variations of stiffness seen in PAH arteries. Using the model, we have shown that PAH-SMC cells are highly susceptible to directional migration. We also showed the utility of this platform by screening different KIs, and the data generated suggests that the JAK/STAT pathway may play a role as a mechanosensor for PAH-SMCs stiffness-induced directional migration.

Directional cell migration is a fundamental process that begins with the sensing of stiffness variations by different cellular mechanosensory machineries. FAK is a crucial regulator of this process, and it is overexpressed in the lungs of patients.[44] However, the transition from FAK activation to the formation of FAK cytoskeletons that interact with the ECM involves the simultaneous activation of multiple pathways. The JAK/STAT and Hippo signaling pathways are two important modulators of cellular migration that also show important functions in PAH-SMC biology.[45–47] The JAK/STAT system is a rapid signaling channel that transmits signals from the cell membrane to the nucleus. It activates the production of essential mediators and plays a role in the stability of microtubules during directional cell migration.[48] While the canonical pathway of MST2 involves the transcriptional inactivation of YAP/TAZ and thus the inhibition of cellular proliferation, previous studies observed no effect of MST1/2 on TAP/TAZ in PAH-SMCs.[49] On the contrary, a non-canonical Hippo/MST-signaling pathway drives the growth and survival of PAH-SMCs.[27] Using KIs, we found that the JAK/STAT and Hippo/MST signaling pathways are involved in the stiffness-induced directional PAH-SMC migration. The JAK/STAT pathway was prioritized over STK/MST despite some kinase inhibitors showing lower DMiX values due to its well-established role in PAH pathophysiology and mechanotransduction. JAK3 exhibited the highest phosphorylation levels in PAH-SMCs, making it a strong candidate for further investigation.[26] This study suggests that the stiffness-induced activation of JAK3/STAT3 represents a useful target to modulate PAH-SMCs directional migration. While STK/MST inhibitors showed promise, their role in stiffness-mediated migration remains less understood, requiring further research. Whether the JAK/STAT and Hippo/MST signaling pathways operate in conjunction or independently during the PAH-SMCs migration also remains unclear. Future studies will be needed to investigate the underlying mechanisms of these pathways and their potential synergistic effects on the collective directional migration of PAH-SMCs.

While we screened a moderate number of compounds in our micropatterned bioengineering platform, our model holds great potential for utility. With the recent advent of 3D-printing techniques, we could scale from the current 24-well-based format to 96-well-based high-throughput platform. The semi-automated method to visualize and count the pre-labeled cells before and after compound screening also makes it feasible to perform the assay robustly. To show the utility of our micropatterned model, we used polyacrylamide as the soft or stiff gel mimicking the stiffness variations of PAH arteries. However, the alternating soft or stiff stripes can be easily fabricated using gels that more closely mimic ECM, such as collagen or laminins, as shown here. Among all PAH cell types, PAH-SMCs demonstrated the highest DMiX, indicating a strong preference for stiffness-driven migration. While overall high trends were observed in stiffness-mediated directional cell migration patterns, some variability existed among patients, which could be attributed to genetic differences, disease severity, and prior treatments. Differences in PAH-SMC behavior suggest that not all patients respond similarly to stiffness-induced migration cues, which could influence therapeutic targeting strategies. Investigating the molecular basis of these variabilities could lead to patient-specific therapeutic strategies, possibly linking mechanosensor activation to genetic or epigenetic differences. We believe our soft-stiff micropatterned model provides a platform that can support ongoing efforts to identify the newfound role of different kinases in the stiffness-induced directional migration of PAH cells and, thus, to further explore their role in PAH arterial remodeling. Screening of different KIs with different cell types, *e.g.*, PAH-SMCs, pericytes, or PAH-ADCs that also show high DMiX in our model, may also identify cell-specific mechanosensors that are involved in directional migration. The hydrogel gradient generated by this micropatterned structure ranges from a few to several hundred kPa,

making it well-suited for replicating the mechanical properties of pathological conditions. The structured or randomized orientations of the soft/stiff gel patterns can be adjusted to mimic the varying diameters of pulmonary arterioles across the proximal, middle, and distal sections by modifying stripe widths. However, further research exploiting a new design that incorporates varying stripe distances, stripe widths, and curvatures can be done in future to study their effects on PAH-SMC cell migration.

Our screening platform is designed to identify kinase inhibitors that target stiffness-induced PAH cell migration—a key process in arterial remodeling in PAH. While sotatercept, an ActRIIA-Fc fusion protein, has demonstrated efficacy in reversing vascular remodeling by neutralizing activin-class ligands and restoring BMP signaling,[50,51] its mechanism appears distinct from that of stiffness-mediated migration. Although activin A has chemotactic effects in immune and stromal cells *via* both canonical (SMAD2/3) and non-canonical (PI3K/Akt, MAPK/ERK) pathways,[52–54] studies indicate that neither activin A nor ActRIIA-Fc ligands influence PAH-SMC migration.[55] This distinction highlights the utility of our platform in dissecting alternative migration-specific signaling pathways, such as JAK/STAT and MST, which are not directly targeted by sotatercept. Therefore, our model could be leveraged to explore combination strategies where sotatercept's antiproliferative effects are complemented by KIs that directly block SMC migration. This approach could provide a synergistic therapeutic benefit by targeting both structural remodeling and the dynamic cellular behaviors driving disease progression in PAH.

In summary, this research underscores the importance of employing innovative bioengineering models to address unresolved issues related to the pathophysiology of PAH driven by ECM stiffness. The stiffening of the ECM may set off a positive feedback loop that favors an enhanced directional cell migration that is documented in PAH pulmonary arterial remodeling. Developing therapeutics that target the stiffness-activated mechanosensors for directional cell migration could play a crucial role in preventing the progression of PAH.

Author contributions

TAA and AH conceived the idea. TI, JH, AH, and TAA planned the experimental designs. TI and JH prepared and optimized the soft/stiff gel micropatterned platform with the help of MH. XZ optimized the time for cell migration study. DD and AH provided the kinase inhibitors. TI, JH, and CG tested drugs on the micropatterned platform. TI performed the western blot analysis. TI, JH, MH, and TAA extensively participated in the results discussion, and all the authors contributed to the manuscript writing, reading and editing. TAA supervised the entire study.

Conflicts of interest

The authors declare no conflict of interest.

Data availability

All data reported in this paper are available in the main article and SI. Supplementary Table 1. PAH cells information; Supplementary Table 2. Compound ID, chemical structures and molecular weight (MW); Supplementary Fig. 1. Study of directional cell migration of PAH-SMCs with different densities; Supplementary Fig. 2. Whole cover slide mapping of directed migration of PAH-SMC through microscopic imaging (1-7 represents images taken from different regions of cover slip); Supplementary Fig. 3. Representative microscopic images showing the DCM of PAH-SMCs for PAA and collagen embedded PAA; Supplementary Fig. 4. Drug screening using the micropatterned soft/stiff gel platform; Supplementary Fig. 5. Relative mRNA expression in scrambled siRNA (mock) and targetJAK3 siRNA transfected PAH-SMCs; Supplementary Fig. 6. Relative mRNA expression in control (scrambled siJAK3) and targetJAK3 siRNA transfected PAH-SMCs; Supplementary Fig. 7. Effect of different concentration of JAK3-in-6 and PF06700841 on directed cellmigration using the micropatterned soft/stiff gel platform; Supplementary Fig. 8. Western blot analysis of the relative expression of phospho JAK3 and STAT3obtained after treating with compounds for 30 minutes with various concentrations (0.5, 1.5, and 5μM); Supplementary Fig. 9. Western blot analysis of the relative expression of phospho JAK3 and STAT3obtained from PAH-SMCs cultured in soft versus stiff gels and treated with JAK3-in-6 (JAK3) andPF06700841 (PF). See DOI: **https://doi.org/10.1039/d5bm00224a**.

Acknowledgements

This study was supported by the PhRMA Foundation Predoctoral Fellowship (Identifier-2024 PDDS 1170794), awarded to Tamanna Islam. Also, grants from the Cardiovascular Medical Research and Education Fund (CMREF) #NAID-20200043, NIH SC1GM144171, NIH R01CA262788, NIH R21CA264627, DoD HT94252410217, DoD STTR Phase II #HT942523C0044, and Lizanell and Colbert Coldwell Foundation NAID20220187 that are awarded to Dr Taslim Al-Hilal. The Structural Genomics Consortium (SGC) is a registered charity (no. 1097737) that receives funds from Bayer AG, Boehringer Ingelheim, Bristol Myers Squibb, Genentech, Genome Canada through Ontario Genomics Institute [OGI-196], EU/EFPIA/OICR/McGill/KTH/Diamond Innovative Medicines Initiative 2 Joint Undertaking [EUbOPEN grant 875510], Janssen, Merck KGaA (aka EMD in Canada and United States), Pfizer, and Takeda.

References

1 M. M. Hoeper, K. Dwivedi, C. Pausch, R. A. Lewis, K. M. Olsson, D. Huscher, *et al.*, Phenotyping of idiopathic pulmonary arterial hypertension: a registry analysis, *Lancet Respir. Med.*, 2022, **10**(10), 937–948.

2 K. Y. Chang, S. Duval, D. B. Badesch, T. M. Bull, M. M. Chakinala, T. De Marco, *et al.*, Mortality in Pulmonary Arterial Hypertension in the Modern Era: Early Insights From the Pulmonary Hypertension Association Registry, *J. Am. Heart Assoc.*, 2022, **11**(9), e024969.
3 Z. Cai, Z. Gong, Z. Li, L. Li and W. Kong, Vascular Extracellular Matrix Remodeling and Hypertension, *Antioxid. Redox Signaling*, 2021, **34**(10), 765–783.
4 R. Zolty, Novel Experimental Therapies for Treatment of Pulmonary Arterial Hypertension, *J. Exp. Pharmacol.*, 2021, **13**, 817–857.
5 A. Wang and D. Valdez-Jasso, Cellular mechanosignaling in pulmonary arterial hypertension, *Biophys. Rev.*, 2021, **13**(5), 747–756.
6 C. D. Hartman, B. C. Isenberg, S. G. Chua and J. Y. Wong, Vascular smooth muscle cell durotaxis depends on extracellular matrix composition, *Proc. Natl. Acad. Sci. U. S. A.*, 2016, **113**(40), 11190–11195.
7 S. Lee, J. Hong and J. Lee, Cell motility regulation on a stepped micro pillar array device (SMPAD) with a discrete stiffness gradient, *Soft Matter*, 2016, **12**(8), 2325–2333.
8 S. P. Singh, M. P. Schwartz, E. Y. Tokuda, Y. Luo, R. E. Rogers, M. Fujita, *et al.*, A synthetic modular approach for modeling the role of the 3D microenvironment in tumor progression, *Sci. Rep.*, 2015, **5**, 17814.
9 S. Wong, W. H. Guo and Y. L. Wang, Fibroblasts probe substrate rigidity with filopodia extensions before occupying an area, *Proc. Natl. Acad. Sci. U. S. A.*, 2014, **111**(48), 17176–17181.
10 C. L. Happe, K. P. Tenerelli, A. K. Gromova, F. Kolb and A. J. Engler, Mechanically patterned neuromuscular junctions-in-a-dish have improved functional maturation, *Mol. Biol. Cell*, 2017, **28**(14), 1950–1958.
11 W. J. Hadden, J. L. Young, A. W. Holle, M. L. McFetridge, D. Y. Kim, P. Wijesinghe, *et al.*, Stem cell migration and mechanotransduction on linear stiffness gradient hydrogels, *Proc. Natl. Acad. Sci. U. S. A.*, 2017, **114**(22), 5647–5652.
12 F. Liu, C. M. Haeger, P. B. Dieffenbach, D. Sicard, I. Chrobak, A. M. Coronata, *et al.*, Distal vessel stiffening is an early and pivotal mechanobiological regulator of vascular remodeling and pulmonary hypertension, *JCI Insight*, 2016, **1**(8), e86987.
13 S. S. Dev, S. A. Z. Abidin, R. Farghadani, I. Othman and R. Naidu, Receptor Tyrosine Kinases and Their Signaling Pathways as Therapeutic Targets of Curcumin in Cancer, *Front. Pharmacol.*, 2021, **12**, 772510.
14 M. Iwai, M. Tulafu, S. Togo, H. Kawaji, K. Kadoya, Y. Namba, *et al.*, Cancer-associated fibroblast migration in non-small cell lung cancers is modulated by increased integrin alpha11 expression, *Mol. Oncol.*, 2021, **15**(5), 1507–1527.
15 D. E. Mason, J. M. Collins, J. H. Dawahare, T. D. Nguyen, Y. Lin, S. L. Voytik-Harbin, *et al.*, YAP and TAZ limit cytoskeletal and focal adhesion maturation to enable persistent cell motility, *J. Cell Biol.*, 2019, **218**(4), 1369–1389.
16 A. Q. Sheikh, A. Misra, I. O. Rosas, R. H. Adams and D. M. Greif, Smooth muscle cell progenitors are primed to muscularize in pulmonary hypertension, *Sci. Transl. Med.*, 2015, **7**(308), 308ra159.
17 K. Yuan, Y. Liu, Y. Zhang, A. Nathan, W. Tian, J. Yu, *et al.*, Mural Cell SDF1 Signaling Is Associated with the Pathogenesis of Pulmonary Arterial Hypertension, *Am. J. Respir. Cell Mol. Biol.*, 2020, **62**(6), 747–759.
18 A. Q. Sheikh, F. Z. Saddouk, A. Ntokou, R. Mazurek and D. M. Greif, Cell Autonomous and Non-cell Autonomous Regulation of SMC Progenitors in Pulmonary Hypertension, *Cell Rep.*, 2018, **23**(4), 1152–1165.
19 R. R. Chandran, Y. Xie, E. Gallardo-Vara, T. Adams, R. Garcia-Milian, I. Kabir, *et al.*, Distinct roles of KLF4 in mesenchymal cell subtypes during lung fibrogenesis, *Nat. Commun.*, 2021, **12**(1), 7179.
20 C. E. Evans, N. D. Cober, Z. Dai, D. J. Stewart and Y. Y. Zhao, Endothelial cells in the pathogenesis of pulmonary arterial hypertension, *Eur. Respir. J.*, 2021, **58**(3), 2003957.
21 J. R. Tse and A. J. Engler, Preparation of hydrogel substrates with tunable mechanical properties, *Curr. Protoc. Cell Biol.*, 2010, **Chapter 10**, Unit 106.
22 B. Diaz-Bello, A. X. Monroy-Romero, D. Perez-Calixto, D. Zamarron-Hernandez, N. Serna-Marquez, G. Vazquez-Victorio, *et al.*, Method for the Direct Fabrication of Polyacrylamide Hydrogels with Controlled Stiffness in Polystyrene Multiwell Plates for Mechanobiology Assays, *ACS Biomater. Sci. Eng.*, 2019, **5**(9), 4219–4227.
23 A. Huttenlocher and A. R. Horwitz, Integrins in cell migration, *Cold Spring Harbor Perspect. Biol.*, 2011, **3**(9), a005074.
24 M. Zhou, Y. Ma, E. C. Rock, C. C. Chiang, K. E. Luker, G. D. Luker, *et al.*, Microfluidic single-cell migration chip reveals insights into the impact of extracellular matrices on cell movement, *Lab Chip*, 2023, **23**(21), 4619–4635.
25 P. Mehta, Z. Rahman, P. Ten Dijke and P. E. Boukany, Microfluidics meets 3D cancer cell migration, *Trends Cancer*, 2022, **8**(8), 683–697.
26 D. Yerabolu, A. Weiss, B. Kojonazarov, M. Boehm, B. C. Schlueter, C. Ruppert, *et al.*, Targeting Jak-Stat Signaling in Experimental Pulmonary Hypertension, *Am. J. Respir. Cell Mol. Biol.*, 2021, **64**(1), 100–114.
27 T. V. Kudryashova, S. Dabral, S. Nayakanti, A. Ray, D. A. Goncharov, T. Avolio, *et al.*, Noncanonical HIPPO/MST Signaling via BUB3 and FOXO Drives Pulmonary Vascular Cell Growth and Survival, *Circ. Res.*, 2022, **130**(5), 760–778.
28 R. Paulin, J. Meloche, A. Courboulin, C. Lambert, A. Haromy, A. Courchesne, *et al.*, Targeting cell motility in pulmonary arterial hypertension, *Eur. Respir. J.*, 2014, **43**(2), 531–544.
29 C. P. Tinworth and R. J. Young, Facts, Patterns, and Principles in Drug Discovery: Appraising the Rule of 5 with Measured Physicochemical Data, *J. Med. Chem.*, 2020, **63**(18), 10091–10108.

30 G. S. Cockerill, R. M. Angell, A. Bedernjak, I. Chuckowree, I. Fraser, J. Gascon-Simorte, *et al.*, Discovery of Sisunatovir (RV521), an Inhibitor of Respiratory Syncytial Virus Fusion, *J. Med. Chem.*, 2021, **64**(7), 3658–3676.

31 S. Seetharaman, B. Vianay, V. Roca, A. J. Farrugia, C. De Pascalis, B. Boeda, *et al.*, Microtubules tune mechanosensitive cell responses, *Nat. Mater.*, 2022, **21**(3), 366–377.

32 B. C. Isenberg, P. A. Dimilla, M. Walker, S. Kim and J. Y. Wong, Vascular smooth muscle cell durotaxis depends on substrate stiffness gradient strength, *Biophys. J.*, 2009, **97**(5), 1313–1322.

33 J. Y. Xu, N. B. Chang, T. Li, R. Jiang, X. L. Sun, Y. Z. He, *et al.*, Endothelial Cells Inhibit the Angiotensin II Induced Phenotypic Modulation of Rat Vascular Adventitial Fibroblasts, *J. Cell. Biochem.*, 2017, **118**(7), 1921–1927.

34 S. Sartore, A. Chiavegato, E. Faggin, R. Franch, M. Puato, S. Ausoni, *et al.*, Contribution of adventitial fibroblasts to neointima formation and vascular remodeling: from innocent bystander to active participant, *Circ. Res.*, 2001, **89**(12), 1111–1121.

35 S. Crnkovic, H. Thekkekara Puthenparampil, S. Mulch, V. Biasin, N. Radic, J. Wilhelm, *et al.*, Adventitial fibroblasts direct smooth muscle cell-state transition in pulmonary vascular disease, *eLife*, 2025, **13**, RP98558.

36 T. Bertero, W. M. Oldham, K. A. Cottrill, S. Pisano, R. R. Vanderpool, Q. Yu, *et al.*, Vascular stiffness mechanoactivates YAP/TAZ-dependent glutaminolysis to drive pulmonary hypertension, *J. Clin. Invest.*, 2016, **126**(9), 3313–3335.

37 O. Boucherat, V. Agrawal, A. Lawrie and S. Bonnet, The Latest in Animal Models of Pulmonary Hypertension and Right Ventricular Failure, *Circ. Res.*, 2022, **130**(9), 1466–1486.

38 T. A. Al-Hilal, A. Keshavarz, H. Kadry, B. Lahooti, A. Al-Obaida, Z. Ding, *et al.*, Pulmonary-arterial-hypertension (PAH)-on-a-chip: fabrication, validation and application, *Lab Chip*, 2020, **20**(18), 3334–3345.

39 A. J. Ainscough, T. J. Smith, M. Haensel, C. J. Rhodes, A. Fellows, H. J. Whitwell, *et al.*, An organ-on-chip model of pulmonary arterial hypertension identifies a BMPR2-SOX17-prostacyclin signalling axis, *Commun. Biol.*, 2022, **5**(1), 1192.

40 S. V. Plotnikov, A. M. Pasapera, B. Sabass and C. M. Waterman, Force fluctuations within focal adhesions mediate ECM-rigidity sensing to guide directed cell migration, *Cell*, 2012, **151**(7), 1513–1527.

41 M. Ehrbar, A. Sala, P. Lienemann, A. Ranga, K. Mosiewicz, A. Bittermann, *et al.*, Elucidating the role of matrix stiffness in 3D cell migration and remodeling, *Biophys. J.*, 2011, **100**(2), 284–293.

42 J. Hui and S. W. Pang, Cell migration on microposts with surface coating and confinement, *Biosci. Rep.*, 2019, **39**(2), BSR20181596.

43 S. C. B. Herath, S. Sharghi-Namini, Y. Du, D. Wang, R. Ge, Q. G. Wang, *et al.*, A Magneto-Microfluidic System for Investigating the Influence of an Externally Induced Force Gradient in a Collagen Type I ECM on HMVEC Sprouting, *SLAS Technol.*, 2017, **22**(4), 413–424.

44 D. Lagares, O. Busnadiego, R. A. Garcia-Fernandez, M. Kapoor, S. Liu, D. E. Carter, *et al.*, Inhibition of focal adhesion kinase prevents experimental lung fibrosis and myofibroblast formation, *Arthritis Rheum.*, 2012, **64**(5), 1653–1664.

45 R. Paulin, J. Meloche and S. Bonnet, STAT3 signaling in pulmonary arterial hypertension, *JAKSTAT*, 2012, **1**(4), 223–233.

46 G. T. K. Boopathy and W. Hong, Role of Hippo Pathway-YAP/TAZ Signaling in Angiogenesis, *Front. Cell Dev. Biol.*, 2019, **7**, 49.

47 J. Park and C. G. Hansen, Cellular feedback dynamics and multilevel regulation driven by the hippo pathway, *Biochem. Soc. Trans.*, 2021, **49**(4), 1515–1527.

48 S. Z. Prisco, L. M. Hartweck, L. Rose, P. D. A. Lima, T. Thenappan, S. L. Archer, *et al.*, Inflammatory Glycoprotein 130 Signaling Links Changes in Microtubules and Junctophilin-2 to Altered Mitochondrial Metabolism and Right Ventricular Contractility, *Circ.:Heart Failure*, 2022, **15**(1), e008574.

49 T. V. Kudryashova, D. A. Goncharov, A. Pena, N. Kelly, R. Vanderpool, J. Baust, *et al.*, HIPPO-Integrin-linked Kinase Cross-Talk Controls Self-Sustaining Proliferation and Survival in Pulmonary Hypertension, *Am. J. Respir. Crit. Care Med.*, 2016, **194**(7), 866–877.

50 M. M. Hoeper, D. B. Badesch, H. A. Ghofrani, J. S. R. Gibbs, M. Gomberg-Maitland, V. V. McLaughlin, *et al.*, Phase 3 Trial of Sotatercept for Treatment of Pulmonary Arterial Hypertension, *N. Engl. J. Med.*, 2023, **388**(16), 1478–1490.

51 M. Humbert, N. W. Morrell, S. L. Archer, K. R. Stenmark, M. R. MacLean, I. M. Lang, *et al.*, Cellular and molecular pathobiology of pulmonary arterial hypertension, *J. Am. Coll. Cardiol.*, 2004, **43**(12 Suppl S), 13S–24S.

52 L. Salogni, T. Musso, D. Bosisio, M. Mirolo, V. R. Jala, B. Haribabu, *et al.*, Activin A induces dendritic cell migration through the polarized release of CXC chemokine ligands 12 and 14, *Blood*, 2009, **113**(23), 5848–5856.

53 Y. Wang, Z. Liu, Y. Qi, J. Wu, B. Liu and X. Cui, Activin A, a Novel Chemokine, Induces Mouse NK Cell Migration via AKT and Calcium Signaling, *Cells*, 2024, **13**(9), 728.

54 L. Jiang, Y. Qi, X. Kong, R. Wang, J. Qi, F. Lin, *et al.*, Activin A as a Novel Chemokine Induces Migration of L929 Fibroblasts by ERK Signaling in Microfluidic Devices, *Front. Cell Dev. Biol.*, 2021, **9**, 660316.

55 L. M. Yung, P. Yang, S. Joshi, Z. M. Augur, S. S. J. Kim, G. A. Bocobo, *et al.*, ACTRIIA-Fc rebalances activin/GDF versus BMP signaling in pulmonary hypertension, *Sci. Transl. Med.*, 2020, **12**(543), eaaz5660.

56 A. Pardanani, T. Lasho, G. Smith, C. J. Burns, E. Fantino and A. Tefferi, CYT387, a selective JAK1/JAK2 inhibitor: in vitro assessment of kinase selectivity and preclinical studies using cell lines and primary cells from polycythemia vera patients, *Leukemia*, 2009, **23**(8), 1441–1445.

57 S. Howard, V. Berdini, J. A. Boulstridge, M. G. Carr, D. M. Cross, J. Curry, *et al.*, Fragment-based discovery of the pyrazol-4-yl urea (AT9283), a multitargeted kinase inhibitor with potent aurora kinase activity, *J. Med. Chem.*, 2009, **52**(2), 379–388.

58 S. Hart, K. C. Goh, V. Novotny-Diermayr, C. Y. Hu, H. Hentze, Y. C. Tan, *et al.*, SB1518, a novel macrocyclic pyrimidine-based JAK2 inhibitor for the treatment of myeloid and lymphoid malignancies, *Leukemia*, 2011, **25**(11), 1751–1759.

59 F. Elwood, D. J. Witter, J. Piesvaux, B. Kraybill, N. Bays, C. Alpert, *et al.*, Evaluation of JAK3 Biology in Autoimmune Disease Using a Highly Selective, Irreversible JAK3 Inhibitor, *J. Pharmacol. Exp. Ther.*, 2017, **361**(2), 229–244.

60 A. Fensome, C. M. Ambler, E. Arnold, M. E. Banker, M. F. Brown, J. Chrencik, *et al.*, Dual Inhibition of TYK2 and JAK1 for the Treatment of Autoimmune Diseases: Discovery of ((S)-2,2-Difluorocyclopropyl)((1 R,5 S)-3-(2-((1-methyl-1 H-pyrazol-4-yl)amino)pyrimidin-4-yl)-3,8-diazabicyclo[3.2.1]octan-8-yl)methanone (PF-06700841), *J. Med. Chem.*, 2018, **61**(19), 8597–8612.

61 L. Ma, J. R. Clayton, R. A. Walgren, B. Zhao, R. J. Evans, M. C. Smith, *et al.*, Discovery and characterization of LY2784544, a small-molecule tyrosine kinase inhibitor of JAK2V617F, *Blood Cancer J.*, 2013, **3**(4), e109.

62 L. Van Rompaey, R. Galien, E. M. van der Aar, P. Clement-Lacroix, L. Nelles, B. Smets, *et al.*, Preclinical characterization of GLPG0634, a selective inhibitor of JAK1, for the treatment of inflammatory diseases, *J. Immunol.*, 2013, **191**(7), 3568–3577.

63 J. Liang, A. van Abbema, M. Balazs, K. Barrett, L. Berezhkovsky, W. Blair, *et al.*, Lead optimization of a 4-aminopyridine benzamide scaffold to identify potent, selective, and orally bioavailable TYK2 inhibitors, *J. Med. Chem.*, 2013, **56**(11), 4521–4536.

64 A. U. Schirmer, L. M. Driver, M. T. Zhao, C. I. Wells, J. E. Pickett, S. N. O'Bryne, *et al.*, Non-canonical role of Hippo tumor suppressor serine/threonine kinase 3 STK3 in prostate cancer, *Mol. Ther.*, 2022, **30**(1), 485–500.

65 F. Fan, Z. He, L. L. Kong, Q. Chen, Q. Yuan, S. Zhang, *et al.*, Pharmacological targeting of kinases MST1 and MST2 augments tissue repair and regeneration, *Sci. Transl. Med.*, 2016, **8**(352), 352ra108.

66 T. Ishizaki, M. Uehata, I. Tamechika, J. Keel, K. Nonomura, M. Maekawa, *et al.*, Pharmacological properties of Y-27632, a specific inhibitor of rho-associated kinases, *Mol. Pharmacol.*, 2000, **57**(5), 976–983.

